Low Ohmic Losses and Mode Selectivity Provided by a Distributed Bragg Reflector for Cavities of Terahertz Gyrotrons

Vitalii I. Shcherbinin , *Senior Member, IEEE*, Manfred Thumm , *Life Fellow, IEEE*, and John Jelonnek , *Senior Member, IEEE*

***Abstract*— A new high-*Q* dielectric-loaded cavity is considered an alternative to conventional cavities for terahertz gyrotrons. The cavity consists of a two-layered distributed Bragg reflector (DBR) resonator jointed to standard input and output cavity sections. The DBR is formed by a cylindrical dielectric tube and a hollow layer. The main function of the DBR is to shield the metal wall of the resonator from the field of the selected operating mode. It is shown that this mode can be efficiently excited by the same electron beam in both the conventional uniform resonator and the DBR resonator. It is found that the mode conversion at the junctions between DBR resonator and standard cavity sections is low, resulting in more than 99% output purity of the operating mode. It is established that the characteristics of both the conventional and dielectric-loaded cavities exhibit similar robustness against dimensional errors. It is shown that, unlike the competing modes, the operating mode benefits from exceptionally low ohmic losses, which favors improved mode selection in the dielectric-loaded cavity. Using the cavity of an existing second-harmonic 0.5-THz gyrotron as an example, it is shown that sapphire DBR makes it possible to increase the ohmic quality factor of the operating mode and gyrotron efficiency by a factor of 8 and 6, respectively.**

***Index Terms*— Bragg reflector, gyrotron, metal cavity, mode selectivity, ohmic losses.**

I. Introduction

OHMIC losses and mode competition are two related fundamental problems, which place a rigid constraint on efficiency and output power of second-harmonic gyrotrons operated in the subterahertz-to-terahertz frequency range [1]. This fact has stimulated theoretical investigations of various types of gyrotron cavities with improved mode selection [2], [3], [4], [5], [6], [7], [8], [9], [10]. Despite this, today, the trend is to use small-diameter conventional cavities having a sparse frequency spectrum of competing modes at the cost of high-power losses by wall heating. In the best available high-frequency second-harmonic gyrotrons, such power losses usually exceed 80% [11], [12], [13], [14].

A known way to reduce power losses by ohmic heating is to introduce additional diffractive (radiation) losses in the gyrotron cavity, thereby increasing the total cavity losses. Additional losses of the gyrotron cavity can be introduced by nonuniform structural elements [2], [10], [15], [16], such as steps, grooves, and absorbing sections. An increase in the total losses of the gyrotron cavity, however, reduces the beam–wave interaction strength. First, this causes an increase in the starting current of the operating mode and thus can make the problem of mode competition even more challenging. Second, this leads to a decrease in the interaction efficiency. Therefore, despite reduced power losses by cavity heating, the resulting improvement of the gyrotron output efficiency can be minor. Moreover, nonuniform structural elements of the gyrotron cavity initiate mode conversion [17], [18], [19], [20], [21], which is usually neglected or estimated by approximate methods in the beam–wave interaction modeling. The mode conversion can initiate a drastic degradation of gyrotron performance [5], [10], [21], including starting current of the operating mode, output efficiency, and output mode purity.

The ohmic and total losses of a metal cavity can be reduced by cooling it down to cryogenic temperatures with the aim of increasing the electrical conductivity of the cavity wall [22]. For the cavity made of oxygen-free copper, as an example, this makes it possible to increase the ohmic quality factor by a factor of 1.7 at the frequency of around 0.5 THz. However, low-frequency cooling requires additional material and energy costs and therefore can reduce the net efficiency of the overall gyrotron installation.

Another way to reduce ohmic losses is to load the gyrotron cavity with a coaxial rod made of ultralow-loss diamond [23], [24], [25]. Such a diamond-loaded cavity is

The work of Vitalii I. Shcherbinin was supported by the Philipp Schwartz Initiative of the Alexander von Humboldt Foundation. The review of this article was arranged by Editor M. Blank. *(Corresponding author: Vitalii I. Shcherbinin.)*

Vitalii I. Shcherbinin is with the Institute for Pulsed Power and Microwave Technology (IHM), Karlsruhe Institute of Technology (KIT), 76131 Karlsruhe, Germany, and also with the National Science Center "Kharkiv Institute of Physics and Technology," 61108 Kharkiv, Ukraine (e-mail: vshch@ukr.net).

Manfred Thumm and John Jelonnek are with the Institute for Pulsed Power and Microwave Technology (IHM), Karlsruhe Institute of Technol-ogy (KIT), 76131 Karlsruhe, Germany.

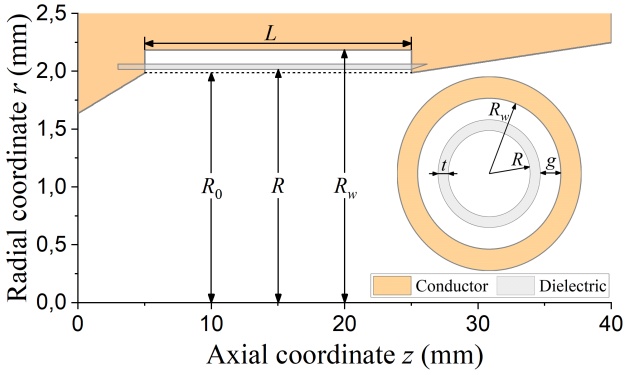

Fig. 1. Structure of a gyrotron cavity with DBR resonator.

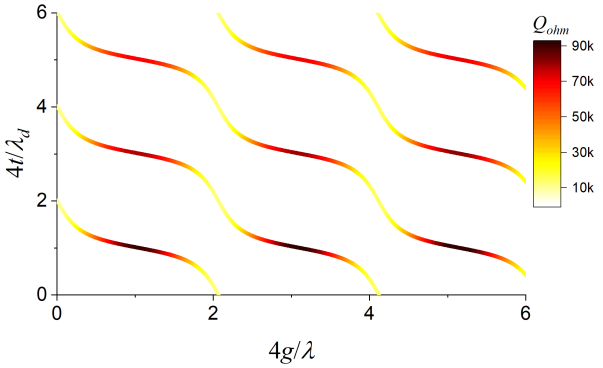

Fig. 2. Dimensional parameters t and g required to support cutoff $TE_{6,n}$ modes with the frequency $f_0 = 526.38$ GHz and ohmic quality factors Q_{ohm} in the dielectric-loaded waveguide with $R = 1.988$ mm, $\sigma = 1.55 \times 10^7$ S/m, $\varepsilon_r = 10$, and $\tan\delta = 5 \times 10^{-5}$.

capable of supporting high-Q modes. These modes are mostly localized inside the diamond rod and therefore can have ohmic quality factors of about 10^5, which is the inverse of the diamond loss tangent at the subterahertz frequencies [26]. Such ohmic quality factors are more than five times higher than those of conventional metal cavities of high-frequency second-harmonic gyrotrons [11], [12], [13], [14]. The main drawback of the diamond-loaded cavity is a fairly close spatial arrangement of the diamond rod and electron beam. Therefore, to maintain high beam–wave interaction strength and to avoid unwanted electron interception by the diamond, strict cavity alignment is required.

A distributed Bragg reflector (DBR) can provide an alternative means of reducing ohmic losses in the metal gyrotron cavity. It is formed by specially sized stacked dielectric layers and is designed to diminish the field amplitude of the operating mode near the conducting cavity wall. In the microwave range, the high-Q DBR resonators find use in many applications [27], [28], [29], including recent experiments on dark-matter axion search [30], [31]. This study considers the potential use of the DBR resonator in a cavity of a second-harmonic gyrotron operated at the frequency of around 0.5 THz. A number of such gyrotrons with conventional cavities have been fabricated worldwide for spectroscopic applications and exhibit an output efficiency below 3% [13], [14], [32], [33].

II. Waveguide Modes

In the analysis of gyrotron cavities, waveguide modes (also known as radial or normal modes) are commonly used to form an orthogonal mode basis. They are eigenmodes of an infinitely long uniform waveguide.

Our prime interest is in eigenmodes of a conducting cylindrical waveguide loaded with a coaxial dielectric tube (see the inset of Fig. 1). The dielectric tube has the inner radius R, thickness t, and relative complex permittivity $\varepsilon = \varepsilon_r(1 + i\tan\delta)$. The wall radius and electrical conductivity of the waveguide are R_w and σ, respectively.

There is a well-established rigorous technique for solving a boundary-value problem for a multilayered dielectric cylinder [34], [35]. The resulting equation is the dispersion relation, which relates the axial wavenumbers k_z and complex frequencies ω of the waveguide modes to the dimensional parameters of the dielectric-loaded waveguide. In the general case, these modes are hybrid modes. The exceptions are axially symmetric ($m = 0$) and cutoff ($k_z = 0$) $TE_{m,n}$ and $TM_{m,n}$ modes.

Gyrotrons operate in TE modes excited near cutoff frequencies $\omega_0 = 2\pi f_0(1 - i/(2Q_{\rm ohm}))$. As an example, we refer to the frequency of 526.38 GHz, which corresponds to the cutoff frequency f_0 of the $TE_{6,5}$ mode of a hollow ($t = 0$) conducting cylindrical waveguide of the radius 1.988 mm. The same radius $R = 1.988$ mm is adopted for the hollow core region of the dielectric-loaded waveguide.

For $\sigma = 1.55 \times 10^7$ S/m, $\varepsilon_r = 10$, and $\tan\delta = 5 \times 10^{-5}$, the capacity of this waveguide to support cutoff $TE_{6,n}$ modes with specified frequency $f_0 = 526.38$ GHz is shown in Fig. 2 as a function of t/λ_d and g/λ, where g is the size of the radial gap between the dielectric tube and conducting waveguide (Fig. 1) and $\lambda = c/f_0$ and $\lambda_d = \lambda/\sqrt{\varepsilon_r}$ are the wavelengths in the hollow (free space) and dielectric-filled regions at 526.38 GHz, respectively. The calculated waveguide modes have the same frequency and field distribution inside the hollow core region ($r < R$) of the dielectric-loaded waveguide. Despite this, they differ widely in ohmic losses, which include wall and dielectric losses. The wall losses are proportional to the skin depth δ_s multiplied by the square of the tangential magnetic field at the conducting wall. The dielectric losses are proportional to the loss tangent $\tan\delta$ multiplied by the electric field energy stored inside the dielectric region [24], [28], [29].

Of all modes in Fig. 2, one can distinguish low-Q and high-Q modes. Low-Q modes correspond to $t \approx i\lambda_d/2$ ($i = 0, 1, 2, \ldots,$) and $g \approx j\lambda/2$ ($j = 0, 1, 2, \ldots,$) and include $TE_{6,n}$ modes supported by the hollow ($t = 0$) conducting waveguide [Fig. 3(a)]. High ohmic quality factors are achieved for $t \approx (2i + 1)\lambda_d/4$ and $g \approx (2j + 1)\lambda/4$ due to the Bragg reflection, which results in reduced magnitude of the tangential magnetic field at the conducting surface $r = R_w$ [Fig. 3(a)]. As the thickness $t \approx (2i + 1)\lambda_d/4$ of the dielectric tube increases with i, the electric field energy stored inside the dielectric region increases, resulting in a decrease in the ohmic quality factors of high-Q waveguide modes (Fig. 2). Despite this fact, in practice, an increase in the dielectric thickness from $t \approx \lambda_d/4$ to $t \approx 3\lambda_d/4$ (or $t \approx 5\lambda_d/4$) can provide a

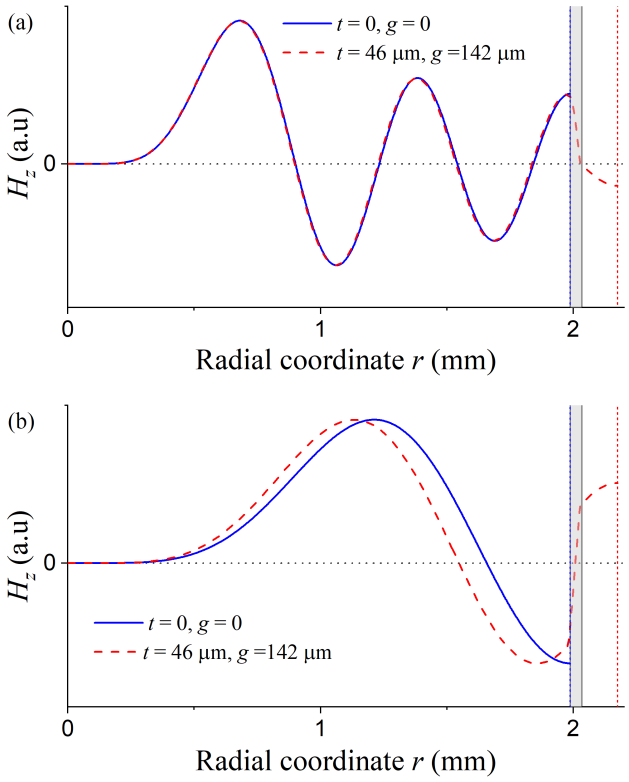

Fig. 3. Radial distribution of the axial magnetic field of the cutoff (a) $TE_{6,5}$ and (b) $TE_{5,2}$ modes in the hollow and dielectric-loaded waveguides. Here, the frequencies and ohmic quality factors of the $TE_{6,5}$ and $TE_{5,2}$ modes of the hollow (dielectric-loaded) waveguide are 526.38 GHz and 10 400 (526.38 GHz and 90 200) and 252.48 GHz and 6050 (269.73 GHz and 8650), respectively.

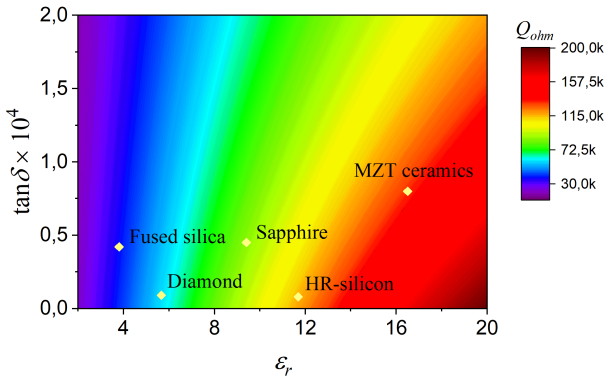

Fig. 4. Ohmic quality factor of the cutoff $TE_{6,5}$ mode with the frequency of 526.38 GHz as a function of the real permittivity ε_r and loss tangent $\tan\delta$ for the dielectric-loaded waveguide with $R = 1.988$ mm, $g = \lambda/4$, and $t \approx \lambda_d/4$. Diamond-shaped markers show ε_r and $\tan\delta$ for chemical vapor deposition diamond [26], fused silica [36], sapphire [36], high-resistivity (HR) silicon [37], and MgO–ZnO–TiO_2 (MZT)-based [38] ceramics at around 0.5 THz.

good tradeoff between performance and manufacturability of the dielectric-loaded waveguide.

Bragg confinement of the waveguide modes can be improved by using a multilayered dielectric DBR [27], [28]. Another way of increasing Q_{ohm} is to make use of high-permittivity dielectric materials [29]. Fig. 4 shows the effect of ε_r and $\tan\delta$ on the ohmic quality factor of the dielectric-loaded waveguide with the gap size $g = \lambda/4 = 142$ μm and dielectric thickness $t \approx \lambda_d/4$, which is adjusted

TABLE I
COLD CHARACTERISTICS OF CONVENTIONAL CAVITY **A**

Mode	Freq. (GHz)	Q_{dif}	Q_{ohm}	Q_{tot}
$TE_{6,5}$	526.40	63200	10400	8900
$TE_{5,2}$	252.56	9970	6070	3770

to support the cutoff $TE_{6,5}$ mode with the frequency of 526.38 GHz. It can be seen that, compared to low-permittivity materials, high-permittivity dielectrics are capable of providing higher ohmic quality factors of the dielectric-loaded waveguide, despite higher material losses. In the following, we will use the parameters $\varepsilon_r = 10$ and $\tan\delta = 5 \times 10^{-5}$, which are close to those of the sapphire at the frequency of 0.5 THz [36]. Clearly, in deciding on the appropriate dielectric material for gyrotron application, additional considerations must be given to its vacuum, thermal, mechanical, machining, and charging properties.

The Bragg reflection is a frequency-dependent phenomenon. Therefore, once the dimensional parameters of the dielectric-loaded waveguide have been optimized to support the high-Q $TE_{6,5}$ mode, other waveguide modes do not gain the same full benefit from the DBR. The dielectric loading affects the frequencies of these modes, along with ohmic losses. This effect can be seen from Fig. 3(b) for the $TE_{5,2}$ mode. In the presence of the DBR, the cutoff frequency and ohmic quality factor of this mode increase from 252.48 and 6050 to 269.73 GHz and 8650, respectively. At the same time, the optimized DBR has only a slight effect on the frequency of the $TE_{6,5}$ mode and initiates a large increase of Q_{ohm} from 10 400 to 90 200. Thus, it furnishes a means for discrimination of waveguide modes by ohmic losses.

In the following, using a fast simplified approach [10], [39], [40], normal hybrid modes of the dielectric-loaded waveguide are used as a basis to calculate cold-cavity characteristics and to model beam–wave interaction in a gyrotron cavity with DBR. In this approach, the widely used self-consistent gyrotron equations for a near-cutoff (quasi-) TE mode are combined with the mode-matching technique. The approach considers the conversion of normal modes due to step discontinuities of the cavity structure. For good numerical convergence, the number of coupled normal modes is taken equal to 30.

III. COLD-CAVITY CALCULATIONS

For reference, let us first consider a conventional all-metal gyrotron cavity referred to as cavity **A**. The cavity has the wall conductivity $\sigma = 1.55 \times 10^7$ S/m and consists of a uniform cylindrical resonator joined to input and output sections. The resonator has the radius $R_0 = 1.988$ mm and the length $L = 20$ mm. The tapering angles of the input and output sections are 4° and 1°, respectively. The cold characteristics of cavity **A** are listed in Table I and are close to those of the cavity of the second-harmonic 0.5-THz gyrotron [14]. For the $TE_{6,5}$ mode supported by this cavity, peak power losses by cavity heating are about 85%.

Cavity **B** is formed from cavity **A** by the replacement of the uniform cylindrical resonator with DBR resonator of the

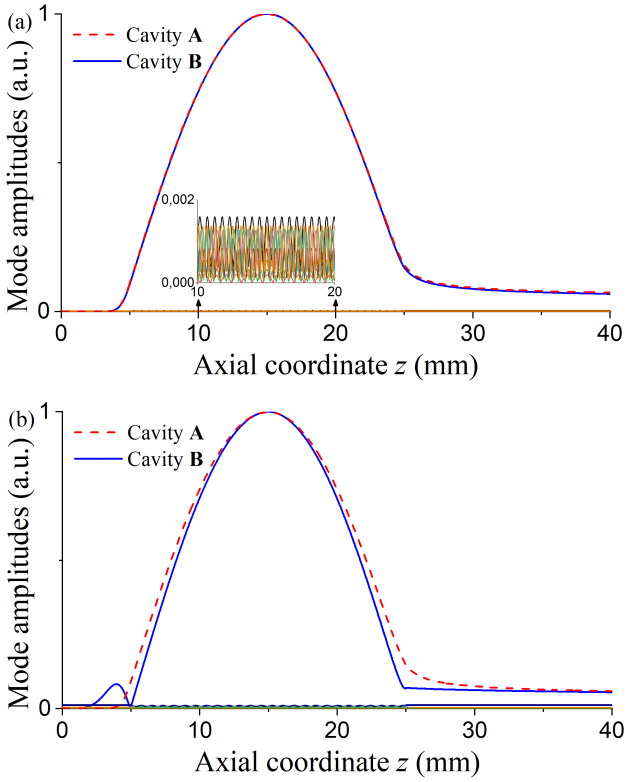

Fig. 5. Cold-cavity field profiles of (a) $TE_{6,5}$ and (b) $TE_{5,2}$ modes of cavities **A** and **B**.

same length $L = 20$ mm. The DBR consists of a dielectric tube with $\varepsilon_r = 10$, $\tan\delta = 5 \times 10^{-5}$, and $t = 46$ μm and a hollow gap with $g = 142$ μm ($R_w = 2.176$ mm). Inside the resonator, the dielectric tube can be held in place by circular grooves carved into metal endplates of the input and output cavity sections, as shown in Fig. 1. Such a holding method for sapphire tubes has been implemented in the microwave range and is characterized by a minor penetration of the electromagnetic field into carved grooves [31].

For simplicity, we first assume zero spacing δR between the inner radius R of the dielectric tube and the radii $R_0 = 1.988$ mm of the metal endplates of the input and output cavity sections (Fig. 1). However, it should be emphasized that, in practice, the requirement $\delta R = 0$ can be hard to fulfill to a high accuracy because of manufacturing errors. Besides, it is desirable to set the spacing δR much larger than the skin depth δ_s in order to prevent field penetration into the dielectric-loaded circular grooves of the input and output cavity sections.

Fig. 5(a) shows the cold-cavity field profiles of the $TE_{6,5}$ mode supported by cavities **A** and **B**. It can be seen that the diffraction losses of cavity **B** are somewhat lower than those of cavity **A**. This is due to increased reflection of the $TE_{6,5}$ mode from the junctions between the DBR resonator and all-metal cavity sections. Since the resonator is not perfectly optimized, it also initiates a slight change in the cold-cavity frequency of the $TE_{6,5}$ mode. It is essential that the nonuniform structure of cavity **B** induces a minor conversion of the $TE_{6,5}$ mode to spurious normal mode [see amplitudes of spurious modes in the inset of Fig. 5(a)]. This is generally in contrast with mode

TABLE II
COLD CHARACTERISTICS OF CAVITY **B** WITH DBR RESONATOR

Mode	Error	Freq. (GHz)	Q_{dif}	Q_{ohm}	Q_{tot}	η_p (%)
$TE_{5,2}$	0	269.93	29200	8630	6660	88.36
$TE_{6,5}$	0	526.42	72200	85300	39100	99.54
δR_w	+2 μm	526.36	72600	85500	39300	99.55
	−2 μm	526.47	71900	85000	39000	99.53
δt	+2 μm	525.92	75300	84800	39900	99.63
	−2 μm	526.91	71500	85300	38900	99.39
δR	+2 μm	525.96	74800	85100	39800	99.61

conversion induced by cavity steps in all-metal cylindrical cavities [10], [17], [18], [21], [40] and can be explained by the fact that the DBR reduces the field strength of the $TE_{6,5}$ mode outside the core region of the gyrotron cavity [Fig. 3(a)]. As a result, the output purity η_p of the $TE_{6,5}$ mode of cavity **B** exceeds 99%. The distinguishing feature of this cavity is low ohmic loss. Because of this, for the $TE_{6,5}$ mode of cavity **B**, the peak power losses by cavity heating are below 46% but can be slightly increased up to 47.5% with the increasing length of the output cavity section. The full list of the cold-cavity characteristics of this mode is given in Table II.

Except for the ohmic quality factor, the cold-cavity characteristics of the $TE_{6,5}$ mode are only slightly affected by the DBR. However, this is not the case for other cavity modes. For the $TE_{5,2}$ mode, as an example, this is evident from Fig. 5(b) and Table II. It can be seen that the DBR profoundly alters the cold-cavity frequency of the $TE_{5,2}$ mode. The frequency change is accompanied by increased reflection of this mode and its conversion into spurious normal modes at the ends of the resonator. These phenomena cause an increase in the diffractive quality factor and a decrease in the output purity of the $TE_{5,2}$ mode. Despite the increase in the diffractive quality factor, the resulting increase in the total quality factor of the $TE_{5,2}$ mode due to the DBR is about 2.5 times lower than that of the $TE_{6,5}$ mode. This demonstrates the mode selectivity provided by the DBR.

As can be seen from Fig. 5(b), the field of the $TE_{5,2}$ mode penetrates into the input section of cavity **B**. A straightforward way to avoid such field penetration is to increase the input tapering angle. This causes a decrease in the interaction cavity length and diffractive quality factor of the $TE_{5,2}$ mode. In this study, however, such additional discrimination against the $TE_{5,2}$ mode will be omitted for the sake of simplicity.

It is well known that manufacturing errors in cavity dimensions can strongly reduce the real benefit from the use of step-shaped cavities in gyrotrons [5], [10], [21], [40]. Therefore, from the practical standpoint, it is essential to demonstrate the robustness of the cavity characteristics to manufacturing errors. Three sorts of dimensional errors of cavity **B** have been considered. The first error is the error δR_w in the radius $R_w = 2.176$ mm $+ \delta R_w$ of the metal wall. The second error is the error δt in the thickness $t = 46$ μm $+ \delta t$ of the dielectric tube. The third error is the abovementioned spacing δR between the inner radius $R = 1.988$ mm $+ \delta R$ of the dielectric tube and the radii $R_0 = 1.988$ mm of the metal endplates of the input and output cavity sections (Fig. 1).

The effect of dimensional errors of cavity **B** on the cold-cavity characteristics of the $TE_{6,5}$ mode is summarized in

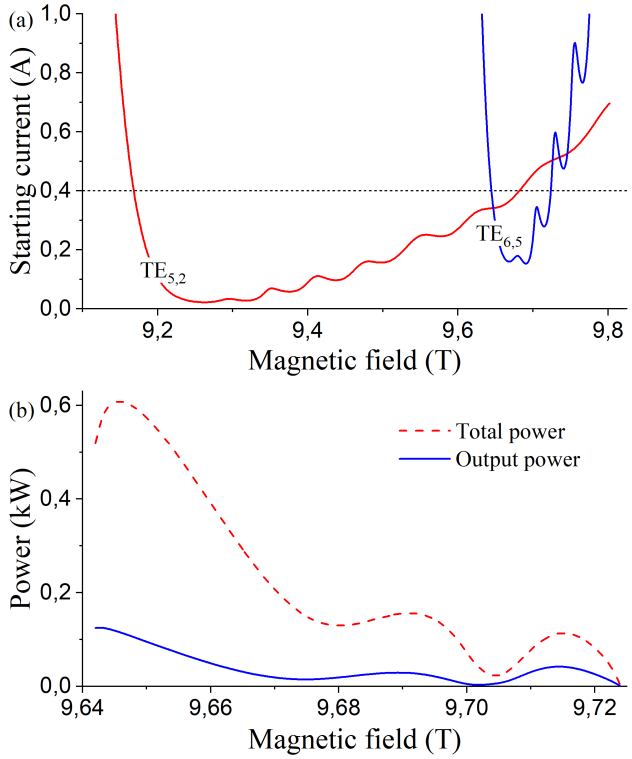

Fig. 6. (a) Starting currents of the second-harmonic $TE_{6,5}$ and first-harmonic $TE_{5,2}$ modes and (b) total and output power of the second-harmonic 0.5-THz gyrotron with cavity **A**.

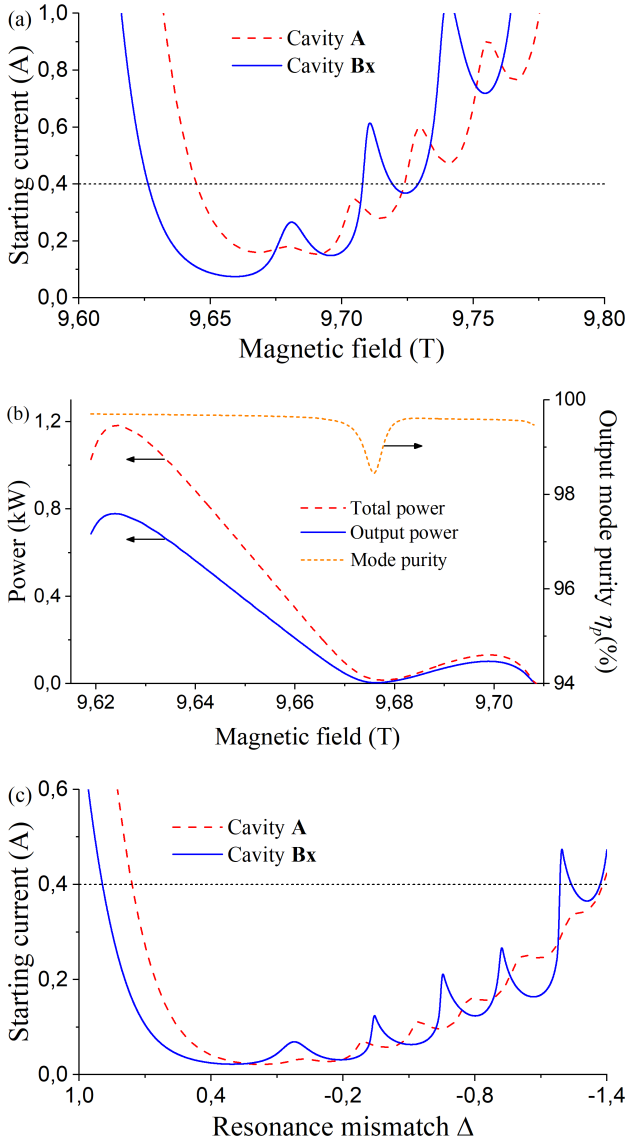

Fig. 7. (a) Starting currents of the $TE_{6,5}$ mode in cavities **A** and **Bx**. (b) Output mode purity, total, and output power of the second-harmonic $TE_{6,5}$ mode of the 0.5-THz gyrotron with cavity **Bx**. (c) Starting currents of the $TE_{5,2}$ mode of cavities **A** and **Bx** versus the resonance mismatch.

Table II. It can be seen that, in all cases of interest, the change in the total quality factor of the $TE_{6,5}$ mode is below 2% and the output mode purity exceeds 99%. The strongest effect is observed for the error $\delta t = \pm 2$ μm, which leads to a frequency shift of 0.5 GHz for the $TE_{6,5}$ mode. Such a frequency shift, however, is not exceptional and is even lower than that induced by a 2-μm error in the radius of the conventional cavity **A** at the frequency of 526.4 GHz. Therefore, similar dimensional accuracy is required for manufacturing of both cavities **A** and **B**.

IV. Beam–Wave Interaction Modeling

Our interest is in the performance of a second-harmonic 0.5-THz gyrotron powered by the electron beam with current $I_b = 0.4$ A, voltage $V_b = 15$ kV, radius $r_b = 0.87$ mm, pitch factor $\alpha = 1.2$, and Gaussian distribution of the transverse electron velocities at the cavity input with the standard deviation $\delta v_\perp = 8\%$. The gyrotron is designed to operate in the $TE_{6,5}$ mode and is initially equipped with conventional cavity **A**. In this cavity, the first-harmonic $TE_{5,2}$ mode is the most dangerous competing mode.

Fig. 6(a) shows the starting currents of the $TE_{6,5}$ and $TE_{5,2}$ modes. It can be seen that the first-harmonic $TE_{5,2}$ mode presents no serious obstacle to single-mode excitation of the operating mode. In the single-mode regime of gyrotron operation, the total power generated by the electron beam and the interaction efficiency can reach 610 W and 10.2%, respectively [Fig. 6(b)]. However, most of the generated power in the all-metal cylindrical cavity is lost by ohmic wall heating. Because of this, the peak output power and efficiency of the second-harmonic 0.5-THz gyrotron equipped with cavity **A** drop to 125 W and 2.1%, respectively.

The operating mode has similar field distribution inside the hollow cores of cavities **A** and **B** [Fig. 3(a)]. Therefore, in cavity **B** with DBR resonator, the operating mode can be excited by the same electron beam that has been used in the conventional cavity 0.5-THz gyrotron. Because of low ohmic losses in this cavity, its length is not optimal for peak output power and requires modification. The modified cavity is designated as cavity **Bx** and has a reduced length $L = 17$ mm of the DBR resonator. In addition, the radii R_0 of the metal endplates of the input and output sections of cavity **Bx** are set equal to 1.986 mm (Fig. 1). This involves a formation of the spacing $\delta R = R - R_0 = 2$ μm, which far exceeds the skin depth $\delta_s = 0.18$ μm of the metal cavity wall.

Fig. 7(a) shows the starting current of the operating $TE_{6,5}$ mode supported by cavities **A** and **Bx**. It can be seen that,

compared to the conventional resonator, the DBR resonator with shorter length L provides a lower minimum starting current of the $TE_{6,5}$ mode. This is because of low total losses of cavity **Bx**. However, this benefit of the DBR resonator is reduced for high-order axial modes, which are characterized by higher diffractive losses. This is why there is a narrowing of the frequency bandwidth of the 0.5-THz gyrotron equipped with the shortened cavity **Bx**.

Fig. 7(b) shows the variation of the total power, output power, and output purity of the operating mode supported by cavity **Bx** along the operating range of the 0.5-THz gyrotron. It can be seen that the use of the DBR in the gyrotron cavity enables nearly twofold increase in the peak total power and interaction efficiency up to 1185 W and 19.7%, respectively. The reason is that a decrease in cavity losses leads to increased strength of the beam–wave interaction [41]. In addition, the peak power losses by ohmic heating of cavity **Bx** amount only to about 34%, including 32% and 2% attributed to losses in metal and dielectric, respectively. As a result, the operating $TE_{6,5}$ mode reaches the output power of 780 W and output efficiency of 13%, which are more than six times higher than those of the 0.5-THz gyrotron with conventional cavity **A** [Fig. 6(b)]. It is significant that, in the presence of the electron beam, the degradation of the output mode purity due to the DBR remains low and is below 2% throughout the entire frequency tuning range of the 0.5-THz gyrotron.

As discussed above, the DBR radically alters the frequency spectrum of competing modes supported by the gyrotron cavity. Therefore, in a practical situation, an additional mode analysis of the DBR resonator may be needed to replace the $TE_{6,5}$ mode with a new operating mode characterized by larger frequency separation from the competing modes. Such an analysis remains to be done in further research.

The effect of the DBR on competing modes is considered by the example of the $TE_{5,2}$ mode. Fig. 7(c) shows the starting currents of the first-harmonic $TE_{5,2}$ mode supported by cavities **A** and **Bx** versus the resonance mismatch $\Delta = 2\beta_{\perp 0}^{-2}(1 - \omega_{c0}/\omega)$, where ω_{c0} and $\beta_{\perp 0}$ are the initial relativistic cyclotron frequency and mean transverse velocity divided by the speed of light in vacuum, respectively. It can be seen that cavities **A** and **Bx** provide a comparable level of the starting current for the competing mode. Therefore, leaving aside the frequency change, we can state that the risk of excitation of the $TE_{5,2}$ mode in cavities **A** and **Bx** is nearly the same. At the same time, cavity **Bx** favors excitation of the operating second-harmonic $TE_{6,5}$ mode having the minimum starting current, which is below one-half that of the operating mode supported by cavity **A** [Fig. 7(a)]. This provides an argument in favor of feasibility of the single-mode operation for high-performance second-harmonic terahertz gyrotrons with high-Q DBR resonators.

V. Conclusion

The DBR formed by a dielectric tube and a hollow layer has been considered as a means of reducing ohmic losses of the selected operating mode in a metal cavity of a terahertz gyrotron. It has been shown that such a reflector optimized to support the operating mode has a minor effect on its frequency and field distribution inside the hollow core of the cavity. Therefore, the same electron beam can be used to excite the operating mode in both a conventional cavity and the cavity with DBR resonator. It has been found that the output purity of the operating mode in the cavity with DBR resonator, which is joined to the standard input and output sections, exceeds 99% and is robust against dimensional errors. The major effect produced by errors is a shift in the operating frequency. This frequency shift has been shown to be close to that induced by a similar error in the radius of the conventional gyrotron cavity. Therefore, no exceptional tolerances are required to manufacture the cavity with DBR resonator for the desired operating frequency. Unlike the conventional cavity, this cavity provides low ohmic losses in the operating mode. This is because the DBR shields the metal cavity wall from the mode field. The larger the real permittivity and the smaller the loss tangent of the dielectric tube, the higher the ohmic quality factor of the operating mode. It has been shown that this can result in a sixfold increase in the gyrotron output power. Since the DBR is optimized to support the operating mode at the desired frequency, its effect on ohmic losses of the competing modes is reduced. In addition, it has been shown that the DBR affects the frequencies of the competing modes and leads to the reflection and conversion of these modes at the resonator ends. This can cause an increase in the diffractive quality factors of the competing modes. It has been shown that, despite this unwanted effect, the gyrotron cavity with DBR resonator can exhibit improved mode selectivity due to low ohmic losses of the operating mode.

References

[1] S. H. Kao, C. C. Chiu, and K. R. Chu, "A study of sub-terahertz and terahertz gyrotron oscillators," *Phys. Plasmas*, vol. 19, no. 2, Feb. 2012, Art. no. 023112, doi: 10.1063/1.3684663.

[2] I. V. Bandurkin, Y. K. Kalynov, and A. V. Savilov, "Klystron-like cavity with mode transformation for high-harmonic terahertz gyrotrons," *Phys. Plasmas*, vol. 20, no. 1, Jan. 2013, Art. no. 014503, doi: 10.1063/1.4775083.

[3] V. I. Shcherbinin and V. I. Tkachenko, "Cylindrical cavity with distributed longitudinal corrugations for second-harmonic gyrotrons," *J. Infr., Millim., Terahertz Waves*, vol. 38, no. 7, pp. 838–852, Jul. 2017, doi: 10.1007/s10762-017-0386-x.

[4] I. V. Bandurkin, M. Y. Glyavin, S. V. Kuzikov, P. B. Makhalov, I. V. Osharin, and A. V. Savilov, "Method of providing the high cyclotron harmonic operation selectivity in a gyrotron with a spatially developed operating mode," *IEEE Trans. Electron Devices*, vol. 64, no. 9, pp. 3893–3897, Sep. 2017, doi: 10.1109/TED.2017.2731982.

[5] M. M. Melnikova et al., "Electromagnetic modeling of a complex-cavity resonator for the 0.4-THz second-harmonic frequency-tunable gyrotron," *IEEE Trans. Electron Devices*, vol. 64, no. 12, pp. 5141–5146, Dec. 2017, doi: 10.1109/TED.2017.2764874.

[6] X. Guan, W. Fu, and Y. Yan, "A 0.4-THz second harmonic gyrotron with quasi-optical confocal cavity," *J. Infr., Millim., Terahertz Waves*, vol. 38, no. 12, pp. 1457–1470, Dec. 2017, doi: 10.1007/s10762-017-0432-8.

[7] V. I. Shcherbinin, V. I. Tkachenko, K. A. Avramidis, and J. Jelonnek, "Coaxial cavity with stepped inner conductor for a sub-terahertz second-harmonic gyrotron with broadband continuous frequency tuning," *IEEE Trans. Electron Devices*, vol. 66, no. 12, pp. 5313–5320, Dec. 2019, doi: 10.1109/TED.2019.2944647.

[8] V. I. Shcherbinin, Y. K. Moskvitina, K. A. Avramidis, and J. Jelonnek, "Improved mode selection in coaxial cavities for subterahertz second-harmonic gyrotrons," *IEEE Trans. Electron Devices*, vol. 67, no. 7, pp. 2933–2939, Jul. 2020, doi: 10.1109/TED.2020.2996179.

[9] V. I. Shcherbinin, "Multifunctional coaxial insert with distributed impedance corrugations for cavities of broadband tunable second-harmonic gyrotrons," *IEEE Trans. Electron Devices*, vol. 68, no. 8, pp. 4104–4109, Aug. 2021, doi: 10.1109/TED.2021.3090348.

[10] V. I. Shcherbinin, T. I. Tkachova, A. V. Maksimenko, M. Thumm, and J. Jelonnek, "A novel complex cavity for second-harmonic subterahertz gyrotrons: A tradeoff between engineering tolerance and mode selection," *J. Infr. Millim. Terahertz Waves*, vol. 43, nos. 11–12, pp. 957–971, Dec. 2022, doi: 10.1007/s10762-022-00888-w.

[11] L. Agusu, T. Idehara, H. Mori, T. Saito, I. Ogawa, and S. Mitsudo, "Design of a CW 1 THz gyrotron (gyrotron Fu Cw III) using a 20 T superconducting magnet," *Int. J. Infr. Millim. Waves*, vol. 28, no. 5, pp. 315–328, May 2007, doi: 10.1007/s10762-007-9215-y.

[12] A. C. Torrezan et al., "Continuous-wave operation of a frequency-tunable 460-GHz second-harmonic gyrotron for enhanced nuclear magnetic resonance," *IEEE Trans. Plasma Sci.*, vol. 38, no. 6, pp. 1150–1159, Jun. 2010, doi: 10.1109/TPS.2010.2046617.

[13] S. K. Jawla, R. G. Griffin, I. A. Mastovsky, M. A. Shapiro, and R. J. Temkin, "Second harmonic 527-GHz gyrotron for DNP-NMR: Design and experimental results," *IEEE Trans. Electron Devices*, vol. 67, no. 1, pp. 328–334, Jan. 2020, doi: 10.1109/TED.2019.2953658.

[14] M. Y. Glyavin et al., "A 250-watts, 0.5-THz continuous-wave second-harmonic gyrotron," *IEEE Electron Device Lett.*, vol. 42, no. 11, pp. 1666–1669, Nov. 2021, doi: 10.1109/LED.2021.3113022.

[15] I. V. Bandurkin, Y. K. Kalynov, P. B. Makhalov, I. V. Osharin, A. V. Savilov, and I. V. Zheleznov, "Simulations of sectioned cavity for high-harmonic gyrotron," *IEEE Trans. Electron Devices*, vol. 64, no. 1, pp. 300–305, Jan. 2017, doi: 10.1109/TED.2016.2629029.

[16] Y. K. Kalynov, I. V. Osharin, and A. V. Savilov, "Stable excitation of higher axial modes in the traveling-wave-tube regime in gyrotron cavities with additional loss elements," *IEEE Trans. Electron Devices*, vol. 68, no. 9, pp. 4717–4722, Sep. 2021, doi: 10.1109/TED.2021.3099765.

[17] O. Dumbrajs and E. Borie, "A complex cavity with mode conversion for gyrotrons," *Int. J. Electron.*, vol. 65, no. 3, pp. 285–295, Sep. 1988, doi: 10.1080/00207218808945230.

[18] D. Wagner, G. Gantenbein, W. Kasparek, and M. Thumm, "Improved gyrotron cavity with high quality factor," *Int. J. Infr. Millim. Waves*, vol. 16, no. 9, pp. 1481–1489, Sep. 1995, doi: 10.1007/BF02274811.

[19] A. V. Maksimenko, G. I. Zaginaylov, and V. I. Shcherbinin, "On the theory of longitudinally inhomogeneous waveguides with impedance walls," *Phys. Particles Nuclei Lett.*, vol. 12, no. 2, pp. 362–370, Mar. 2015, doi: 10.1134/S1547477115020168.

[20] A. V. Maksimenko, V. I. Shcherbinin, and V. I. Tkachenko, "Coupled-mode theory of an irregular waveguide with impedance walls," *J. Infr., Millim., Terahertz Waves*, vol. 40, no. 6, pp. 620–636, Jun. 2019, doi: 10.1007/s10762-019-00589-x.

[21] A. V. Maksimenko, V. I. Shcherbinin, A. V. Hlushchenko, V. I. Tkachenko, K. A. Avramidis, and J. Jelonnek, "Starting currents for eigenmodes of a gyrotron cavity with mode conversion," *IEEE Trans. Electron Devices*, vol. 66, no. 3, pp. 1552–1558, Mar. 2019, doi: 10.1109/TED.2019.2893888.

[22] V. E. Zapevalov, A. S. Zuev, V. V. Parshin, E. S. Semenov, and E. A. Serov, "Reduction of ohmic losses in the cavities of low-power terahertz gyrotrons," *Radiophys. Quantum Electron.*, vol. 64, no. 4, pp. 240–250, Sep. 2021, doi: 10.1007/s11141-021-10127-2.

[23] V. I. Shcherbinin, K. A. Avramidis, M. Thumm, and J. Jelonnek, "Mode discrimination by lossy dielectric rods in cavities of second-harmonic gyrotrons," *J. Infr., Millim., Terahertz Waves*, vol. 42, no. 1, pp. 93–105, Jan. 2021, doi: 10.1007/s10762-020-00760-9.

[24] V. I. Shcherbinin, K. A. Avramidis, I. G. Pagonakis, M. Thumm, and J. Jelonnek, "Large power increase enabled by high-Q diamond-loaded cavities for terahertz gyrotrons," *J. Infr., Millim., Terahertz Waves*, vol. 42, no. 8, pp. 863–877, Aug. 2021, doi: 10.1007/s10762-021-00814-6.

[25] V. I. Shcherbinin, K. A. Avramidis, M. Thumm, and J. Jelonnek, "Design of a high-Q diamond-loaded cavity for a third-harmonic subterahertz gyrotron driven by a low-power electron beam," *IEEE Trans. Electron Devices*, vol. 69, no. 6, pp. 3386–3392, Jun. 2022, doi: 10.1109/TED.2022.3166125.

[26] V. V. Parshin, M. Y. Tretyakov, M. A. Koshelev, and E. A. Serov, "Modern resonator spectroscopy at submillimeter wavelengths," *IEEE Sensors J.*, vol. 13, no. 1, pp. 18–23, Jan. 2013, doi: 10.1109/JSEN.2012.2215315.

[27] C. A. Flory and R. C. Taber, "High performance distributed Bragg reflector microwave resonator," *IEEE Trans. Ultrason., Ferroelectr., Freq. Control*, vol. 44, no. 2, pp. 486–495, Mar. 1997, doi: 10.1109/58.585133.

[28] J. Krupka, M. E. Tobar, J. G. Hartnett, D. Cros, and J. M. L. Floch, "Extremely high-Q factor dielectric resonators for millimeter-wave applications," *IEEE Trans. Microw. Theory Techn.*, vol. 53, no. 2, pp. 702–712, Feb. 2005, doi: 0.1109/TMTT.2004.840572.

[29] J.-M. Le Floch, M. E. Tobar, D. Cros, and J. Krupka, "Low-loss materials for high Q-factor Bragg reflector resonators," *Appl. Phys. Lett.*, vol. 92, no. 3, Jan. 2008, Art. no. 032901, doi: 10.1063/1.2828025.

[30] B. T. McAllister, G. Flower, L. E. Tobar, and M. E. Tobar, "Tunable supermode dielectric resonators for axion dark-matter haloscopes," *Phys. Rev. Appl.*, vol. 9, no. 1, Jan. 2018, Art. no. 014028, doi: 10.1103/PhysRevApplied.9.014028.

[31] D. Alesini et al., "Realization of a high quality factor resonator with hollow dielectric cylinders for axion searches," *Nucl. Instrum. Methods Phys. Res. Sect. A, Accel., Spectrometers, Detect. Associated Equip.*, vol. 985, Jan. 2021, Art. no. 164641, doi: 10.1016/j.nima.2020.164641.

[32] M. Blank, S. Cauffman, K. Felch, and P. Borchard, "Development of high-frequency continuous-wave gyrotrons for dynamic nuclear polarization," in *Proc. IEEE 2nd Ukrainian Microw. Week (UkrMW)*, Nov. 2022, pp. 230–233, doi: 10.1109/UkrMW58013.2022.10036954.

[33] T. Song et al., "Experimental investigations on a 500 GHz continuously frequency-tunable gyrotron," *IEEE Electron Device Lett.*, vol. 42, no. 8, pp. 1232–1235, Aug. 2021, doi: 10.1109/LED.2021.3092379.

[34] C. Yeh and G. Lindgren, "Computing the propagation characteristics of radially stratified fibers: An efficient method," *Appl. Opt.*, vol. 16, no. 2, pp. 483–493, 1977, doi: 10.1364/AO.16.000483.

[35] V. I. Shcherbinin, G. I. Zaginaylov, and V. I. Tkachenko, "Analogy between circular core-cladding and impedance waveguides and their membrane functions," *Prog. Electromagn. Res. M*, vol. 53, pp. 111–120, 2017, doi: 10.2528/PIERM16110902.

[36] N. Chudpooti et al., "Wideband dielectric properties of silicon and glass substrates for terahertz integrated circuits and microsystems," *Mater. Res. Exp.*, vol. 8, no. 5, May 2021, Art. no. 056201, doi: 10.1088/2053-1591/abf684.

[37] M. N. Afsar and H. Chi, "Millimeter wave complex refractive index, complex dielectric permittivity and loss tangent of extra high purity and compensated silicon," *Int. J. Infr. Millim. Waves*, vol. 15, no. 7, pp. 1181–1188, Jul. 1994, doi: 10.1007/BF02096073.

[38] S. Wang, Q. Li, J. Gu, J. Han, and W. Zhang, "Dielectric properties of MgO–ZnO–TiO_2-based ceramics at 1 MHz and THz frequencies," *J. Mater. Sci.*, vol. 52, no. 16, pp. 9335–9343, Aug. 2017, doi: 10.1007/s10853-017-1138-y.

[39] A. W. Fliflet, R. C. Lee, and M. E. Read, "Self-consistent field model for the complex cavity gyrotron," *Int. J. Electron.*, vol. 65, no. 3, pp. 273–283, Sep. 1988, doi: 10.1080/00207218808945229.

[40] V. I. Shcherbinin, T. I. Tkachova, M. Thumm, and J. Jelonnek, "Self-consistent modeling of beam-wave interaction in complex gyrotron cavities with azimuthal slots," in *Proc. IEEE 2nd Ukrainian Microw. Week*, Nov. 2022, pp. 258–262, doi: 10.1109/UkrMW58013.2022.10037054.

[41] V. I. Shcherbinin, A. V. Hlushchenko, A. V. Maksimenko, and V. I. Tkachenko, "Effect of cavity ohmic losses on efficiency of low-power terahertz gyrotron," *IEEE Trans. Electron Devices*, vol. 64, no. 9, pp. 3898–3903, Sep. 2017, doi: 10.1109/TED.2017.2730252.